








Spectroscopic Detection of Alfvénic Waves in the Chromosphere of Sunspot Regions

Jongchul Chae¹ , Kyuhyoun Cho¹ , Valery M. Nakariakov^{2,3} , Kyung-Suk Cho^{4,5} , and Ryun-Young Kwon⁴ 

¹Astronomy Program, Department of Physics and Astronomy, Seoul National University, Seoul 08826, Republic of Korea

²Centre for Fusion, Space and Astrophysics, Physics Department, University of Warwick, Coventry CV4 7AL, UK

³School of Space Research, Kyung Hee University, Yongin 17104, Republic of Korea

⁴Solar and Space Weather Group, Korea Astronomy and Space Science Institute, Daejeon 34055, Republic of Korea

⁵Department of Astronomy and Space Science, University of Science and Technology, Daejeon 305-348, Republic of Korea

Received 2021 May 4; revised 2021 May 25; accepted 2021 May 25; published 2021 June 10

Abstract

Transverse magnetohydrodynamic waves often called Alfvénic (or kink) waves have been often theoretically put forward to solve the outstanding problems of the solar corona like coronal heating, solar wind acceleration, and chemical abundance enhancement. Here we report the first spectroscopic detection of Alfvénic waves around a sunspot at chromospheric heights. By analyzing the spectra of the H α line and Ca II 854.2 nm line, we determined line-of-sight velocity and temperature as functions of position and time. As a result, we identified transverse magnetohydrodynamic waves pervading the superpenumbral fibrils. These waves are characterized by the periods of 2.5 to 4.5 minutes, and the propagation direction parallel to the fibrils, the supersonic propagation speeds of 45 to 145 km s⁻¹, and the close association with umbral oscillations and running penumbral waves in sunspots. Our results support the notion that the chromosphere around sunspots abounds with Alfvénic waves excited by the mode conversion of the upward-propagating slow magnetoacoustic waves.

Unified Astronomy Thesaurus concepts: Sunspots (1653); Magnetohydrodynamics (1964); Alfvén waves (23); Solar chromosphere (1479); Solar atmosphere (1477)

Supporting material: animation

1. Introduction

Alfvénic waves are the transverse magnetohydrodynamic waves that propagate along magnetic field lines, referring both incompressive Alfvén waves and compressive kink waves. In a rarefied magnetized plasma, the Alfvénic waves can efficiently carry plasma energy and electromagnetic energy at large distances along magnetic field lines. On the Sun, the Alfvénic waves propagating upward from the low solar atmosphere have been often theoretically invoked to solve the outstanding problems of the solar corona like coronal heating (Alfvén 1947; Osterbrock 1961), solar wind acceleration (Alazraki & Couturier 1971; Belcher 1971), and chemical abundance difference between the photosphere and the corona (Laming 2004). A number of studies reported observational data that are indicative of the presence of Alfvénic waves in various features of the solar atmosphere: the off-limb corona (Tomczyk et al. 2007), off-limb spicules (De Pontieu et al. 2007; He et al. 2009), off-limb prominences (Okamoto et al. 2007), and on-disk chromospheric features of the quiet Sun (Jess et al. 2009).

In the chromosphere of sunspot regions, slow magnetoacoustic waves propagating upward were clearly recognized from the observations of umbral flashes (Beckers & Tallant 1969), umbral oscillations (Giovanelli 1972), and running penumbral waves (Zirin & Stein 1972). The detection of Alfvénic waves in the sunspot chromosphere, however, started recently. Pietarila et al. (2011) reported the first observations of kink waves in a sunspot region. They measured the transverse displacements of a dynamic fibril by analyzing high-resolution intensity data of the Ca II 8542 line. Using the same kind of data and the same method, Morton et al. (2021) systematically investigated more events in superpenumbral fibrils and provided statistical properties of over 2000 transverse motions to find distributions for periods and amplitudes.

So far the detection of the Alfvénic waves has been based on the imaging method that measures the displacements of thread-like features and the oscillations of transverse velocity on the image plane that is perpendicular to the line of sight. This imaging-based detection clearly demonstrates the power of high-resolution intensity data in the study of waves in the solar atmosphere. This technique, however, has limitations as well. Most of all, as thread-like features well separated from others are needed, the detection of oscillations and waves cannot but be selective, being limited to the positions where well-resolved threads exist. Moreover, this technique does not provide any information on the oscillation of line-of-sight velocity at all, so may fail to detect Alfvénic waves that oscillate in the line-of-sight direction only. The line-of-sight velocity can be studied only using the spectroscopic method. This method was previously employed for the detection of Alfvénic waves in the off-limb observations of the corona (Tomczyk et al. 2007), but has not been used in the on-disk observations of the chromosphere.

In this Letter, for the first time, we present the spectroscopic detection of Alfvénic waves pervading the chromosphere of sunspot regions. We infer the line-of-sight velocity from the spectra of the H α line and the Ca II 854.2 nm line. Moreover, since we have a time sequence of raster scans of the spectral data, we obtain line-of-sight velocity at every point in the observed field of view, and at every instant. The resulting three-dimensional arrays of velocity depending on two spatial coordinates in the plane of the sky and time can be readily used for the investigation of the spatio-temporal pattern of velocity and the identification of oscillations and waves. These kinds of data were quite suited for the investigation of transverse waves with line-of-sight velocity oscillations.

2. Data and Methods

We use the spectral data of the $H\alpha$ line and the Ca II 854.2 nm line taken by the Fast Imaging Solar Spectrograph (FISS) of the 1.6 m Goode Solar Telescope at the Big Bear Solar Observatory. The FISS is a dual-band Echelle spectrograph that can record both the $H\alpha$ spectrograms and the Ca II line spectrograms simultaneously with two cameras (Chae et al. 2013). The imaging is achieved by raster scanning, that is, by taking a series of the spectrograms with the slit moving step by step across the field of view. The images at the selected wavelengths are constructed from the raster scan data. The quality of imaging depends on the imaging quality of the light fed into the spectrograph during the scan, which is determined the atmospheric seeing and the performance of the adaptive optics in the telescope.

The specific data used for the current work were the same as those previously used in Chae et al. (2014) taken at 18:50 UT on 2013 July 17. The exposure time for each spectrogram was 30 ms. The spectral sampling and the spectral coverage was 0.0019 and 0.97 nm in the $H\alpha$ line spectra, and 0.0026 and 1.3 nm in the Ca II line spectra. All of the slit width, the step size in the raster scan, and the sampling along the slit were set to $0''.16$. Each raster scan consisted of 250 steps. The observed field of view is $40''$ by $40''$. The observations were done with the 308 subaperture adaptive optics. The spatial resolution of imaging on this day is estimated at twice the step size, which is $0''.32$. The raster scan was repeated for 44 minutes at a cadence of 35 s.

Both the $H\alpha$ line and the Ca II 854.2 nm line are very strong, and are formed throughout the low solar atmosphere, with their continua and far wings being formed in the photosphere, and their cores being formed in the upper chromosphere. In order to derive the physical parameters from the spectra of the lines, we adopt the technique of multilayer spectral inversion (Chae et al. 2020). This technique yields the estimates of eight free parameters from each line profile. They are four source function parameters, two line-of-sight velocity parameters, and the two Doppler width parameters. The source functions are used to construct the maps of photospheric intensity and the line core intensity that are free from the Doppler effect. The line-of-sight velocity of the top layer is the most important parameter for the study of oscillations and waves in the chromosphere. In addition, the Doppler widths of the two lines in the top layers can be combined to yield the estimates of temperature and the most probable speed of nonthermal motion (see Chae et al. 2020 for details). Note that the spectral inversion itself does not provide any information on the atmospheric height of the top layer. Accordingly, we simply suppose that it occupies a part lying between 1000 and 4000 km above the solar surface, where the lower bound is taken to be equal to half of 2000 km, an approximate top height of the average quiet chromosphere, and the upper bound, to be equal to the top height of active region fibrils estimated by Foukal (1971).

The magnetic data used in the present work are the line-of-sight magnetograms taken at 19:36 UT on 2013 July 17 by the HMI instrument on board the Solar Dynamics Observatory. Because the region of our interest was not far from the center of the solar disk, we identified the line-of-sight magnetic field with the vertical component of magnetic field on the solar surface. We have extrapolated the magnetic field on the solar surface to the three-dimensional volume above the surface by

assuming that the magnetic fields in this volume are linear force free. The linear-force-free extrapolation was implemented with the Green function method (Chiu & Hilton 1977). The force-free parameter was chosen so that the constructed field lines in the superpenumbral region are best aligned the $H\alpha$ fibrils when projected on the image plane. We simply take that the $H\alpha$ fibrils trace local magnetic field lines as has been commonly assumed for a long time (Foukal 1971), even though there was an interesting report that Ca II 854.2 nm line fibrils do not always trace magnetic fields (de la Cruz Rodríguez & Socas-Navarro 2011). As the force-free parameter was found to be small, the constructed linear-force-free fields are quite close to the potential magnetic fields.

3. Results

Not surprisingly, we find from the map of line-of-sight velocity (top left of Figure 1) that the chromosphere of the sunspots abounds with velocity oscillations, mostly representing umbral oscillations and penumbral running waves that are well known. The velocity fluctuations have an rms value of 0.9 km s^{-1} over the field of view. In the sunspot umbra around point A (top right of Figure 1), magnetic fields are almost vertical, and the vertical oscillations are parallel to magnetic fields. These oscillations are the well-known umbral oscillations. At regions around point B, which is at the sunspot's periphery, magnetic fields are highly inclined from the vertical and the velocity oscillations propagate outward from the sunspots. These correspond to the running penumbral waves.

Our new finding is that the velocity oscillations in the region of lengthy superpenumbral fibrils (around points C and D) are distinct from the above sunspot oscillations in several ways. We identify these as Alfvénic waves. Most of all, these oscillations are likely to represent velocity oscillations perpendicular to local magnetic fields because the magnetic fields are almost horizontal there. The extrapolated magnetic field lines (middle right and bottom of Figure 1) indicate that the fibrils show up at the regions where significantly horizontal low-lying magnetic field lines exist. Next, these velocity oscillations propagate parallel to the fibrils. This can be inferred from the shape of the regular velocity patches of the same sign seen in the velocity map. We find that these patches are the most elongated in the direction parallel to the fibrils. This implies that the wavelength is the longest in this direction and the oscillations propagate parallel to the fibrils. The length of a velocity patch is as large as 9000 km, based on which we estimate the wavelength roughly at 18,000 km. Finally, these velocity oscillations propagate at supersonic speeds. We estimate the phase speed roughly at 67 to 120 km s^{-1} by adopting the above estimate of wavelength and the oscillation period of 2.5 to 4.5 minutes (to be shown below).

A more rigorous estimate of the propagation speed can be obtained from the spacetime plots of velocity oscillations (left panel of Figure 2) constructed along the predefined cut parallel to the fibrils (top and middle panels of Figure 1). From the slopes of individual streaks of velocity in the plot, we found that the phase speed ranges mostly from 40 to 150 km s^{-1} with a mean of about 90 km s^{-1} and a standard deviation of 45 km s^{-1} . These values are in agreement with the above rough estimate. About 80% of the velocity oscillations are seen to propagate outward from the sunspot center, and about 20% inward. These speeds of propagation are much higher than 14 km s^{-1} , the sound speed estimated with the measured

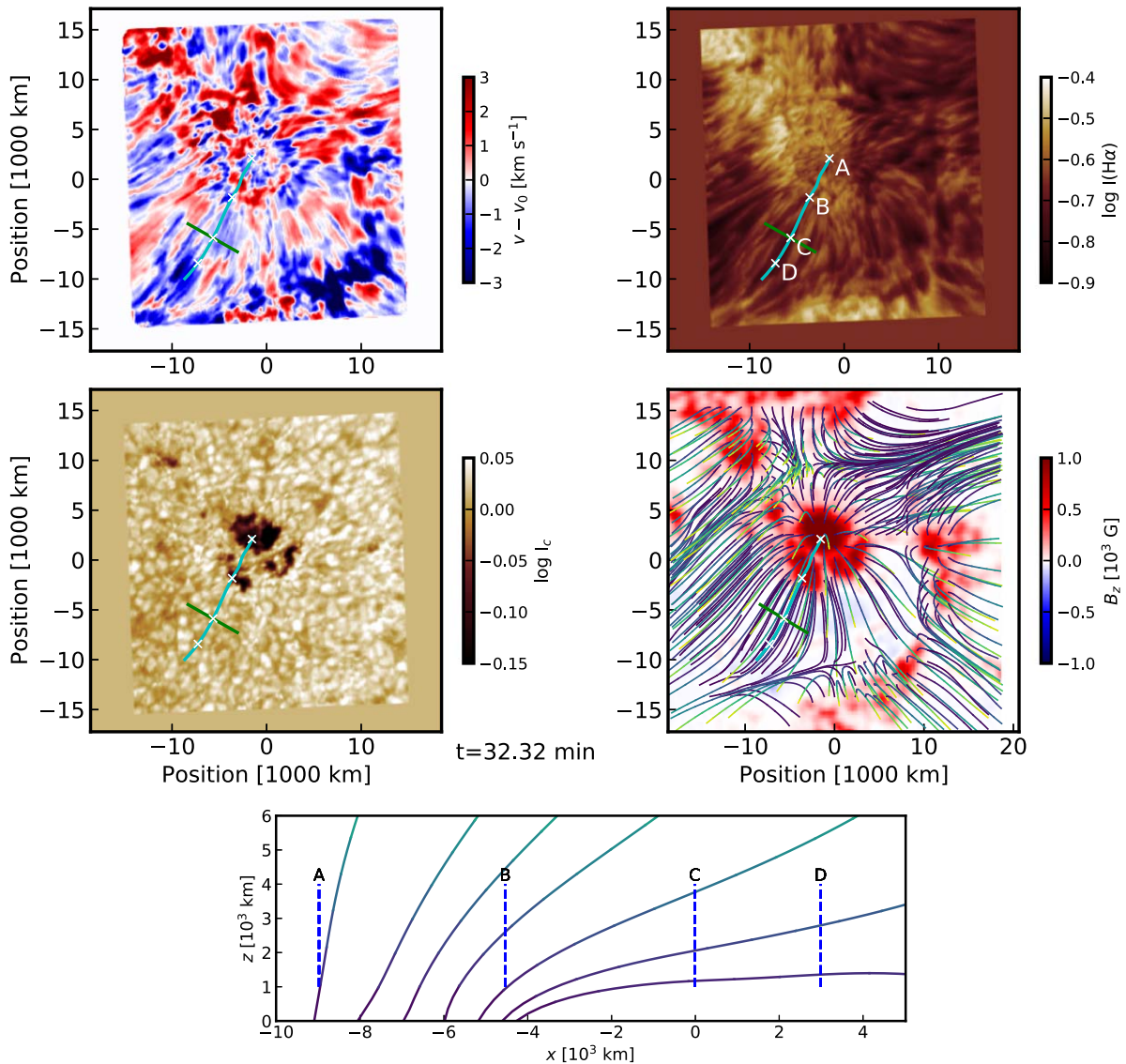


Figure 1. Maps of line-of-sight velocity (upper left), $H\alpha$ line center intensity (upper right), continuum intensity (middle left) constructed from a single raster scan observation of the FISS, and the line-of-sight magnetogram (middle right) with the lines of extrapolated linear-force-free magnetic fields projected on the observing plane. The lower-lying parts of the field lines are marked in darker colors, and the upper-lying parts in brighter colors. Note that the velocity data presented in the map have been high-pass filtered for oscillations of period < 16 minutes. The cyan curve in each map represents the original cut used for the construction of the spacetime plots, and the green line in each map does another cut perpendicular to the original slit. The point of intersection is used to define the origin of the localized Cartesian coordinates for the measurement. The x coordinate increases to the lower left along the cyan curve, and the y coordinate, to the lower right along the green curve. The four locations of interest are marked by the symbols. Bottom: the side view of the extrapolated magnetic field lines. Each vertical dashed line indicates the x value and the supposed z range (1000 to 4000 km) in each location. An animation of the top four panels is available. The animation runs from $t = 0$ to 44.43 minutes. The realtime duration of the animation is 75 s.

(An animation of this figure is available.)

temperature 13,000 K and the assumed mean molecular weight 0.9.

We also find that the velocity oscillations were not confined to a single fibril, but prevailed in the superpenumbral region containing a number of fibrils. From the spacetime plots of velocity constructed along the cut in the direction perpendicular to the fibrils (right panel of Figure 2), we find a series of spatially extended velocity streaks of the same sign that have widths as large as 5000 km, being much broader than the individual fibrils. These streaks are not regular, but look bumpy or fragmented, probably because of the variation of the arrival time over the cut and the inhomogeneities of the medium. The existence of these streaks is strong support that the velocity

oscillations of the same origin prevailed in the area spanning a number of fibrils.

We estimate the primary periods of the velocity oscillations at points C and D at 2.5 to 4.5 minutes from the local peaks of power in the wavelet power spectra of velocity (Figure 3). These periods are close to those of 2.5 to 3.5 minutes at point A and those of 3.5 to 4.5 minutes at point B. Interestingly, we also find secondary oscillations of period around 10 minutes in the wavelet power spectrum at point C. This period is close to the predominant periods of 8 to 10 minutes previously reported for the highly dynamic superpenumbral fibrils located in the other region of the same sunspots (Chae et al. 2014). We conjecture that these longer-period velocity oscillations of smaller

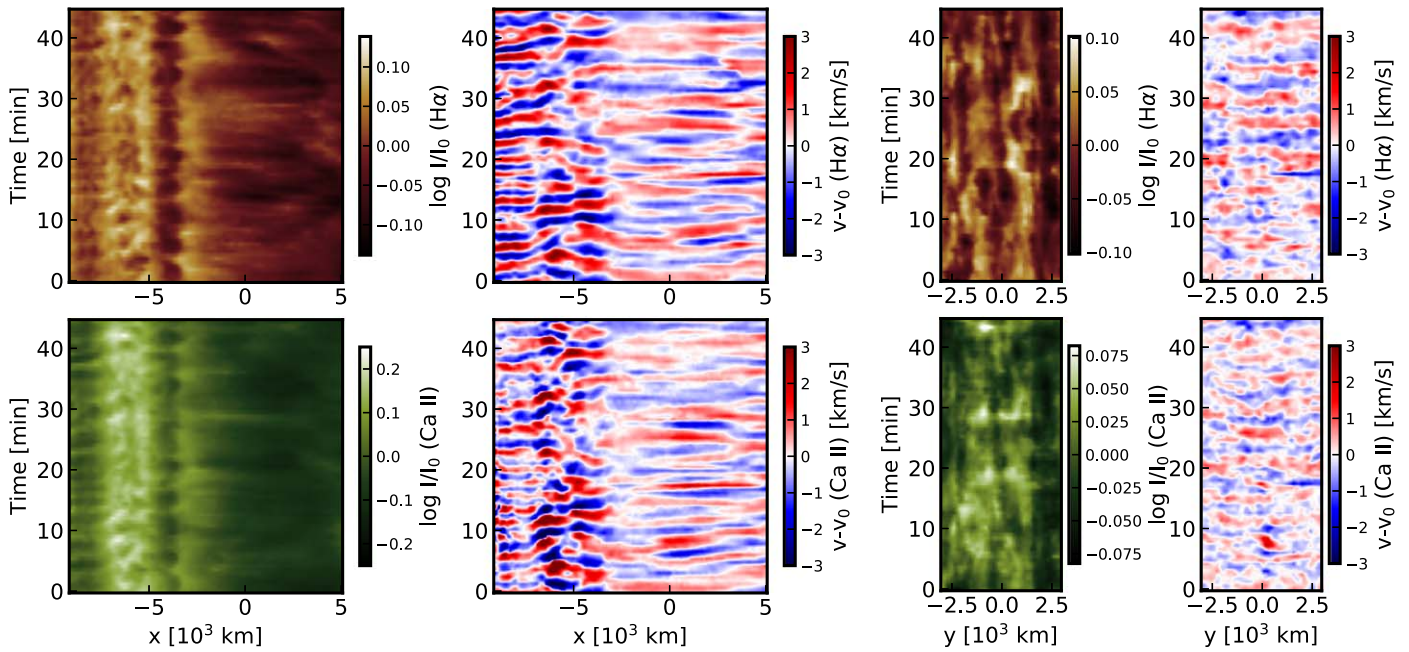


Figure 2. Spacetime plots of line center intensity and line-of-sight velocity in the $H\alpha$ line (upper) and the Ca II line at 854.2 nm (lower) constructed along the original cut (left) and those constructed along its perpendicular cut (right). Note that the velocity data have been high-pass filtered for oscillations of period < 16 minutes, but the intensity data have not.

amplitudes may represent the contribution of field-aligned velocity oscillations to the line-of-sight velocity. This secondary component is not clear at point D.

We acquired observational evidence that the primary oscillations in the fibril region are practically incompressive. We first note that at points A and B, the velocity oscillations are strongly correlated with the temperature oscillations (upper panels of Figure 3) with a small phase difference. This kind of correlation is exactly what is theoretically expected for the slow magnetoacoustic waves nonlinearly propagating in a gravitationally stratified medium (Chae & Litvinenko 2017). At points C and D, such strong correlation does not exist (lower panels of Figure 3). In this region, too, we see a series of peaks in the temperature variation. However, the time interval between the successive temperature peaks is not regular unlike the cases of A and B. We suggest that the temperature peaks are indicative of slow magnetoacoustic shock waves, as can be inferred from the cases of A and B. These supposed slow magnetoacoustic shock waves, however, contribute little to the line-of-sight velocity because the magnetic field lines are very much inclined to the horizontal, i.e., perpendicular to the line of sight, and the slow waves are to involve the field-aligned velocity oscillations only. The observed line-of-sight velocity in points C and D may be mostly due to the velocity oscillations perpendicular to the fields. The lack of strong correlation between velocity and temperature is evidence for the existence of incompressive or weakly compressive velocity oscillations in points C and D.

4. Discussion

The observational properties described above strongly suggest that the velocity oscillations in the fibril region may represent the vertically polarized waves of Alfvénic type propagating along almost horizontal magnetic fields. By identifying the measured propagation speeds of 40 to 150 km s^{-1} with the local Alfvén speed, and by adopting the

magnetic field of about 110 G at heights of 2000 to 4000 km determined from the extrapolated field, we estimate the mass density of the observed region at 0.35 to $5.0 \times 10^{-8} \text{ kg m}^{-3}$. Then, from the observationally inferred velocity amplitude of 1.0 km s^{-1} , we obtain the estimate of 0.26 to 1.0 kW m^{-2} for the wave energy flux. These values are of the same order of magnitude as the value of 0.45 to 2.6 kW m^{-2} , an estimate of acoustic wave energy flux of umbral oscillations (Chae et al. 2019).

We emphasize that ours is the first spectroscopic detection of the Alfvénic waves in the chromosphere of sunspots. We measured the line-of-sight velocities, whereas the previous studies measured lateral displacements of thread-like features. On disk observations, our spectroscopic detection reveals the Alfvénic waves with vertical velocity oscillations and the imaging-based detection does those with horizontal velocity oscillations. If the Alfvénic waves are fully polarized in the vertical direction, they can be detected only through the spectroscopic method. If they are fully polarized in the horizontal direction, they can be detected only through the imaging method. In other cases, they can be detected through both the methods in principle. It was reported that the Alfvénic waves detected with the image method have a wave energy flux of 0.08 to 1.2 kW m^{-2} (Morton et al. 2021), which is very comparable to our estimates. This coincidence suggests that the Alfvénic waves detected by the spectroscopic method are not fully distinct from the Alfvénic waves detected by the imaging method.

Our results suggest that the Alfvénic waves prevalent in the superpenumbral fibrils were excited in close association with the slow magnetoacoustic waves manifest as the umbral oscillations and the penumbral waves. We propose a model of the slow-to-Alfvénic mode conversion that can explain for the excitation of the vertically polarized Alfvénic waves. In this model, vertical field-aligned motions associated with the slow waves in the lower layers are transformed into vertical

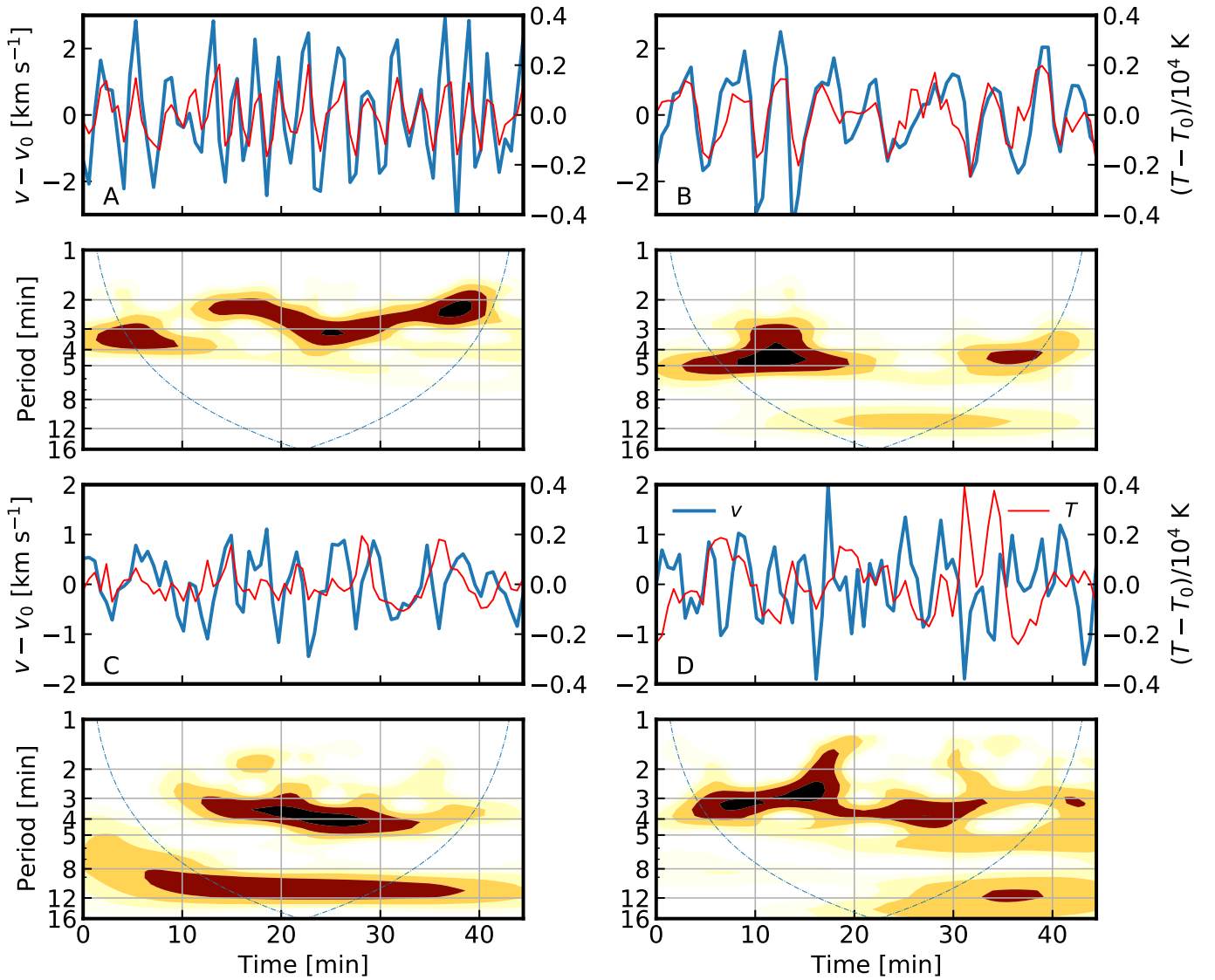


Figure 3. Temporal variations of line-of-sight velocity (blue) and relative temperature fluctuation (red), and the wavelet power spectrum of velocity at points A (upper left), B (upper right), C (lower left), and D (lower right). Both the velocity data and the relative temperature fluctuation have been high-pass filtered for oscillations of period <16 minutes.

perpendicular motions associated with Alfvénic waves in the upper layers. The key element of this model is that the almost vertical field lines in the lower layers bend to almost horizontal field lines in the upper layers. If the radius of curvature is small enough, i.e., much smaller than the wavelength of the waves and the field lines are vertical in the lower layers, and horizontal in the upper layers, the magnetic flux tube could be considered as a right-angled flux slab as depicted in Figure 4. Initially this slab is in magnetohydrostatic equilibrium. When the upflow phase of the slow wave arrives at the bending point at $t = t_0$, the plasma motion carries the field lines upward. This causes a local distortion of field lines and compresses both field lines and plasma at the interface. This field line distortion as well as the compression creates the magnetohydrodynamic force—the force of magnetic tension and the force of total pressure gradient. Similarly, the arrival of the downflow phase at the bend point at $t = t_1$ creates the force directed upward. Thus the period of this oscillating force must be the same as that of the driving slow wave, as further demonstrated by the two times $t = t_2$ and $t = t_3$. Note that the times t_0 , t_1 , t_2 , and t_3

have been introduced to explain the different stages of the process suggested by our observations, but cannot be directly compared with our observations at different times. This interesting task requires new observations with higher time resolution, and more careful data analysis.

This oscillating force can generate two kinds of waves. One is the transverse waves that are mostly driven by the force of magnetic tension and propagate along the field lines. These are the Alfvénic waves. These waves are basically compressive kink waves (see, e.g., Nakariakov & Kolotkov 2020), which is a special kind of fast magnetoacoustic wave guided along the flux slab because of the local nonuniformity of the fast speed across the flux slab. In the special case where compression is insignificant, the Alfvénic waves behave like incompressive Alfvén waves. The other kind of generated waves is the longitudinal waves that are driven by the total pressure gradient, and propagate along the direction of perturbation. These are the leaky fast magnetoacoustic waves as modeled in Nisticò et al. (2014). These waves, however, may not be what

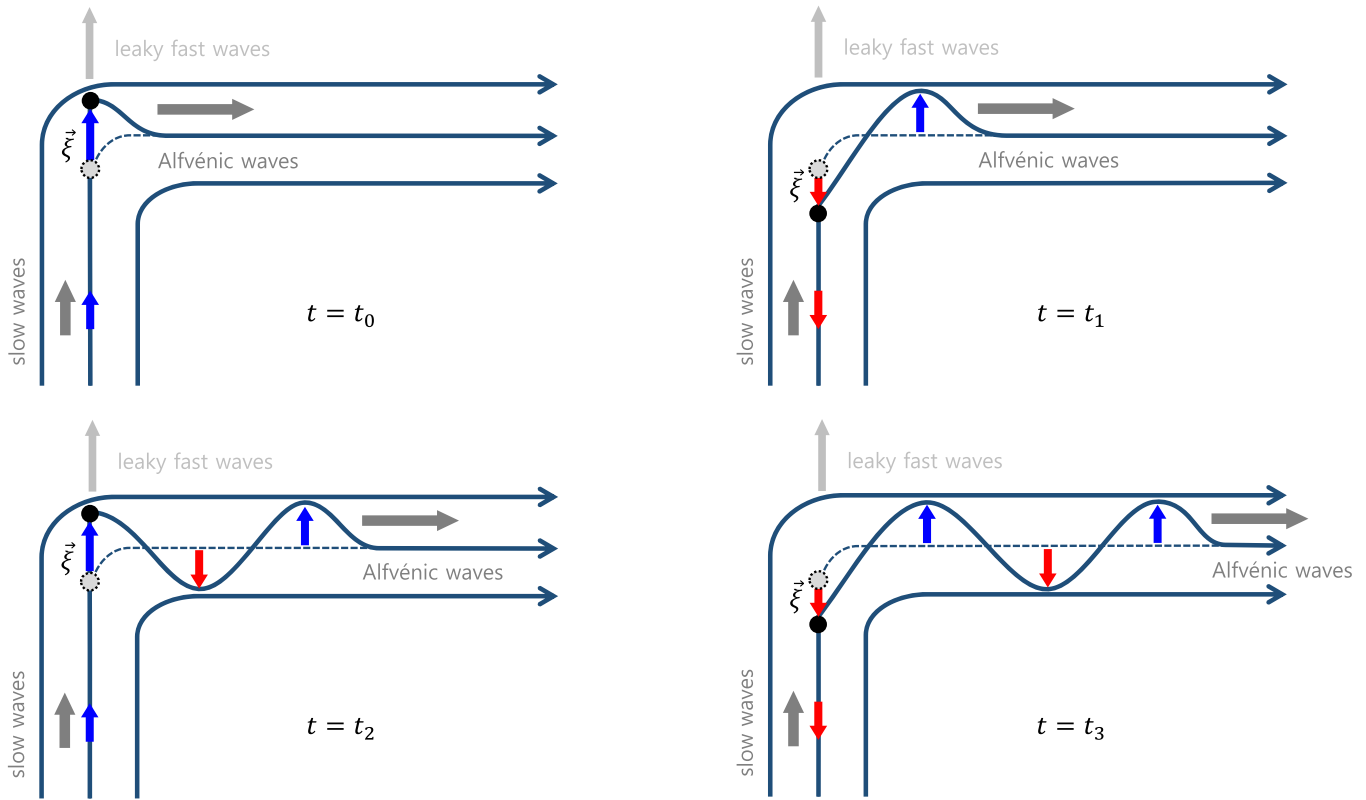


Figure 4. Time series of cartoons illustrating the driving of Alfvénic waves by the mode conversion of slow magnetoacoustic waves at the bend point of the magnetic field lines. The displacement vectors ξ are shown as the arrows.

we observed, because, if any, they may propagate fast out of the flux sheet and the fibrils.

In the above simplified picture of the slow-to-Alfvénic mode conversion, all the slow waves in the low layers are almost converted to the Alfvénic waves at the bending point if the leaky waves are insignificant. In a real situation, however, the bending will occur not with a right angle, but with a larger angle, so we expect that the slow waves will be partly converted to the Alfvénic wave, and the remaining part will keep propagating into the upper part of the flux slab. Furthermore, the realistic bending of the flux tube will occur smoothly with a finite radius of curvature that may be comparable to the wavelength, which will also lead to the gradual and partial conversion of the slow waves into the Alfvénic waves. Accordingly, we predict that in general the upper part of a bent flux slab may host both the transverse Alfvénic waves and the longitudinal slow waves together. The decomposition between the longitudinal slow waves and the transverse Alfvénic waves will be a great challenge for the study of the waves in the solar chromosphere.

This research was supported by the National Research Foundation of Korea (NRF-2020R1A2C2004616 and NRF-2020R1I1A1A01068789). V.M.N. acknowledges support from the STFC consolidated grant ST/T000252/1. The GST operation is partly supported by the Korea Astronomy and Space Science Institute, the Seoul National University, and the Key Laboratory of Solar Activities of Chinese Academy of Sciences (CAS) and the Operation, Maintenance and Upgrading Fund of CAS for Astronomical Telescopes and Facility Instruments.

ORCID iDs

Jongchul Chae <https://orcid.org/0000-0002-7073-868X>
 Kyuhyoun Cho <https://orcid.org/0000-0001-7460-725X>
 Valery M. Nakariakov <https://orcid.org/0000-0001-6423-8286>
 Kyung-Suk Cho <https://orcid.org/0000-0003-2161-9606>
 Ryun-Young Kwon <https://orcid.org/0000-0002-2106-9168>

References

- Alazraki, G., & Couturier, P. 1971, *A&A*, **13**, 380
 Alfvén, H. 1947, *MNRAS*, **107**, 211
 Beckers, J. M., & Tallant, P. E. 1969, *SoPh*, **7**, 351
 Belcher, J. W. 1971, *ApJ*, **168**, 509
 Chae, J., Kang, J., & Litvinenko, Y. E. 2019, *ApJ*, **883**, 72
 Chae, J., & Litvinenko, Y. E. 2017, *ApJ*, **844**, 129
 Chae, J., Madjarska, M. S., Kwak, H., & Cho, K. 2020, *A&A*, **640**, A45
 Chae, J., Park, H.-M., Ahn, K., et al. 2013, *SoPh*, **288**, 1
 Chae, J., Yang, H., Park, H., et al. 2014, *ApJ*, **789**, 108
 Chiu, Y. T., & Hilton, H. H. 1977, *ApJ*, **212**, 873
 de la Cruz Rodríguez, J., & Socas-Navarro, H. 2011, *A&A*, **527**, L8
 De Pontieu, B., McIntosh, S. W., Carlsson, M., et al. 2007, *Sci*, **318**, 1574
 Foukal, P. 1971, *SoPh*, **20**, 298
 Giovanelli, R. G. 1972, *SoPh*, **27**, 71
 He, J. S., Tu, C. Y., Marsch, E., et al. 2009, *A&A*, **497**, 525
 Jess, D. B., Mathioudakis, M., Erdélyi, R., et al. 2009, *Sci*, **323**, 1582
 Laming, J. M. 2004, *ApJ*, **614**, 1063
 Morton, R. J., Moorooogen, K., & Henriques, V. M. J. 2021, *RSPTA*, **379**, 20200183
 Nakariakov, V. M., & Kolotkov, D. Y. 2020, *ARA&A*, **58**, 441
 Nisticò, G., Pascoe, D. J., & Nakariakov, V. M. 2014, *A&A*, **569**, A12
 Okamoto, T. J., Tsuneta, S., Berger, T. E., et al. 2007, *Sci*, **318**, 1577
 Osterbrock, D. E. 1961, *ApJ*, **134**, 347
 Pietarila, A., Aznar Cuadrado, R., Hirzberger, J., & Solanki, S. K. 2011, *ApJ*, **739**, 92
 Tomczyk, S., McIntosh, S. W., Keil, S. L., et al. 2007, *Sci*, **317**, 1192
 Zirin, H., & Stein, A. 1972, *ApJL*, **178**, L85